# J8.5 MOUNTAIN WAVE STRUCTURES OCCURRING WITHIN A MAJOR OROGRAPHIC PRECIPITATION EVENT: PART I. ANALYSES OF AIRBORNE DOPPLER RADAR DATA

Bradley F. Smull, M.F. Garvert and C.F. Mass
Department of Atmospheric Sciences, University of Washington, Seattle, WA, 98195, USA

## 1. INTRODUCTION

The second phase of the Improvement of Microphysical PaRameterization through Observational Verification Experiment (IMPROVE-2) provided a unique opportunity to examine microphysical processes over topography and assess the validity of present day numerical model BMPs. The IMPROVE-2 field experiment, which took place in November and December 2001 over the Oregon Cascades (Fig. 1a) collected a comprehensive set of observations that provided a detailed depiction of the thermodynamic and kinematic structure of many precipitation events (Stoelinga et al. 2003). The collection of kinematic and thermodynamic data simultaneously with microphysical measurements permits a unique opportunity to isolate potential problems in the model BMP from other possible model errors in the dynamic representation of the storm systems.

An exceptional resource to map detailed flow structure within precipitation-laden layers over complex terrain is airborne Doppler radar. IMPROVE-II is one of only two experiments [the other being e.g. MAP (Bousquet and Smull (2003a)] in which airborne Doppler radar data were systematically collected during passage of precipitating cloud systems over a large mountain barrier. The 13-14 December event was particularly well suited to such an exploration because: (a) systematically designed flight tracks were repeated on both the windward and leeward sides of the Cascade crest (Fig. 1b), providing multiple views of the slowly evolving flow/precipitation structure across the barrier, and (b) the extension of detectable radar echo into the lee of the Cascades allowed unusually complete illumination of the subsiding branch of the mountain wave circulation.

The 13-14 December 2001 storm system has already been extensively analyzed in a variety of papers (Garvert et al. 2005a,b, Colle et al. 2005, Woods et al. 2005). The present paper will build upon this foundation by providing a detailed view of the three-dimensional kinematic and reflectivity fields from the Willamette Valley (~100 km upstream of the Cascade crest) to the lee slopes. This paper will utilize the unique dual-Doppler dataset to assess qualitatively the amplitude and strength of mountain waves on several distinct scales over both the lee and windward slopes from a fully three-dimensional perspective. Details of the precipitation pattern,

Corresponding author's address: Bradley Smull, University of Washington Seattle, WA, 98195, USA; E-Mail: smull@atmos.washington.edu

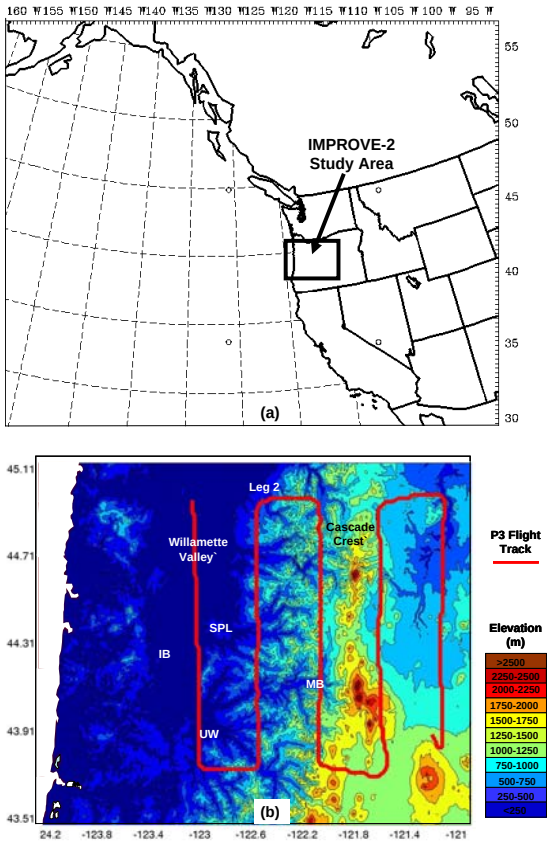


Figure 1. (a) Map of the Pacific Northwest with the IMPROVE-2 study area delineated by box. (b) Elevation map of the IMPROVE-2 study area with flight track of NOAA-P3 (solid red line) overlain. Locations of the sounding site (UW), profiler (IB), vertically pointing NOAA-ETL S-band (MB), and NCAR-S-pol Radar (SPL) are also indicated.

especially as they relate to various mountain wave structures embedded within the flow, will be examined.

## 2. COMPOSITE AIRBORNE DOPPLER ANALYSIS

The capability of airborne dual-Doppler radar to map 3D wind fields over complex terrain has been previously demonstrated (Bousquet and Smull 2003a,b, Yu and Smull 2000). Using the fore- and aft-scanning technique ("FAST"; Frush et al. 1986, Jorgenson and Smull 1993) 3D-reflectivity data for the two-hour period from 2300 UTC 13 December through 0100 UTC 14 December 2001 were gathered in approximately 40 km wide volumes centered along five N-S oriented flight legs (Fig.1b). Each of the individual legs was flown at a constant altitude and

approximately 130-140 km in length, with ~20 km spacing between legs in the cross-barrier (i.e. east-west) direction. Each leg took approximately 30 minutes to complete.

The regular spacing of these five legs provided continuous, overlapping dual-Doppler coverage over the sizable IMPROVE-2 study area, and was thus extremely well suited for evaluation of terrain-modified airflow and precipitation processes via construction of a large composite-type analysis enveloping the Cascades. While airborne Doppler measurements are generally regarded as quantitatively useful to a range of ~40 km, the relatively tight spacing of the P3 legs allowed restriction of analyzed data to a zone within ~20 km on either side (i.e. east and west) of each track, assuring a high-fidelity analysis.

Prior to interpolation, radial velocity and reflectivity measurements were subjected to a combination of automated and manual editing as described by Bousquet and Smull (2003a) to remove ground clutter contamination, noise and other artifacts. Radial data were then interpolated to composite Cartesian grid measuring ~240 km x 170 km in the horizontal with 1 km resolution in x and y and 0.25 km in the vertical, from immediately above the variable terrain surface to a maximum height of 10 km MSL (or echo top, if lower). Multiple radial views from subsequent 'fore' and 'aft' scans were synthesized following Jorgensen and Smull (1993) to yield continuous fields of horizontal airflow (U,V) and reflectivity (dBZ) in regions of detectable echo. Synthesized reflectivity and component airflow fields were subjected to a two-pass Liese filter to eliminate poorly-resolved smaller scale features and to assure smooth, continuous transitions across "seams" separating data from individual flight legs. The absence of notable discontinuities at these locations speaks to the success of this approach.

The resulting composite analysis utilized in this study provides a uniquely expansive and largely uninterrupted view of kinematic and precipitation fields fully spanning the Cascade crest, extending from the Willamette Valley (located >100 km upstream) eastward to the lee-side desert plateau in central Oregon. Due to the slow observed evolution of flow and precipitation structures during this P3 sampling period (Garvert et al. 2005b), the composite analysis may be viewed as a steady-state depiction of the precipitation and flow pattern characterizing the entire 2-hour period.

## 3. OBSERVED FLOW KINEMATICS OVER THE OREGON CASCADES

### *3.1 Windward Slopes*

At a height of 1.5-km, the Doppler measurements showed southwesterly flow exceeding 30 m $s^{-1}$ over the Willamette Valley (Fig. 2a). As this flow encountered the higher terrain of the Cascade foothills, a pronounced deceleration and slight deflection of the winds to a more southerly direction

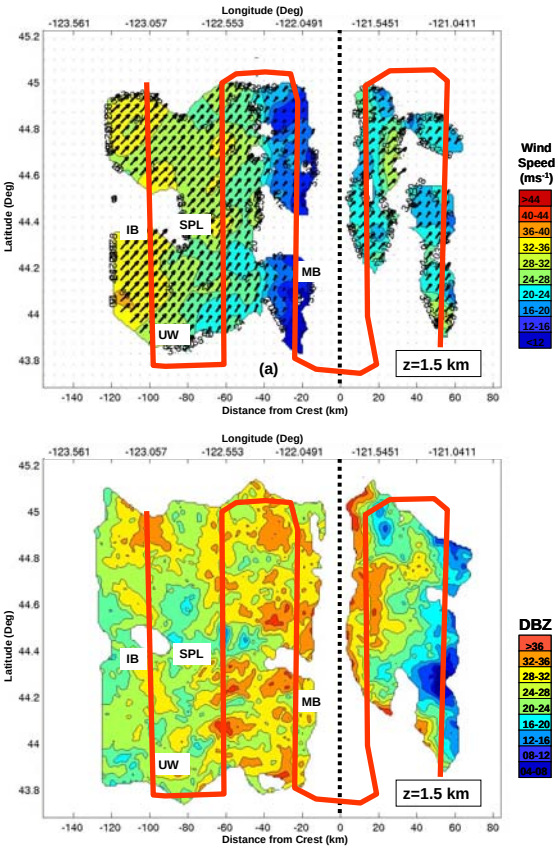


Figure 2. Composite grid of (a) P3 dual-Doppler wind speed (m $s^{-1}$ color shading) and wind vectors and (b) radar reflectivity at elevations of 1.5-km. Red line indicates flight track of P3 over the two-hour period from 2300-0100 UTC 13-14 December 2001.

occurred. Observed reflectivity showed high dBZ values over the entire study area, with pockets of enhanced reflectivity over the windward slopes and a significant reduction in values to the lee (Fig. 2b). Averaged east-west cross sections of U- and V-winds were created to provide a general view of the kinematic fields across the crest of the Cascades (Fig.3 a,b). These sections were developed by averaging the gridded 1-km dual-Doppler data over the full 140-km north-south extent of the domain between 44.0$^0$N and 45.0$^0$N.

Airborne dual-Doppler data indicated the incoming flow was strongly sheared upwind of the crest, with the U-component increasing more than 20 m $s^{-1}$ from between the surface to the top of the shear layer at approximately 2 km (Fig. 3a). A sloping layer of strong vertical shear blanketed the windward slopes, with the depth of this layer remaining relatively constant. The U-profiles over the windward slopes differed from cases of more profoundly blocked flow, as observed adjacent to taller mountain ranges such as the Sierras (Marwitz 1987) and Alps (Medina et al. 2005, Bousquet and Smull 2003b). In those cases the

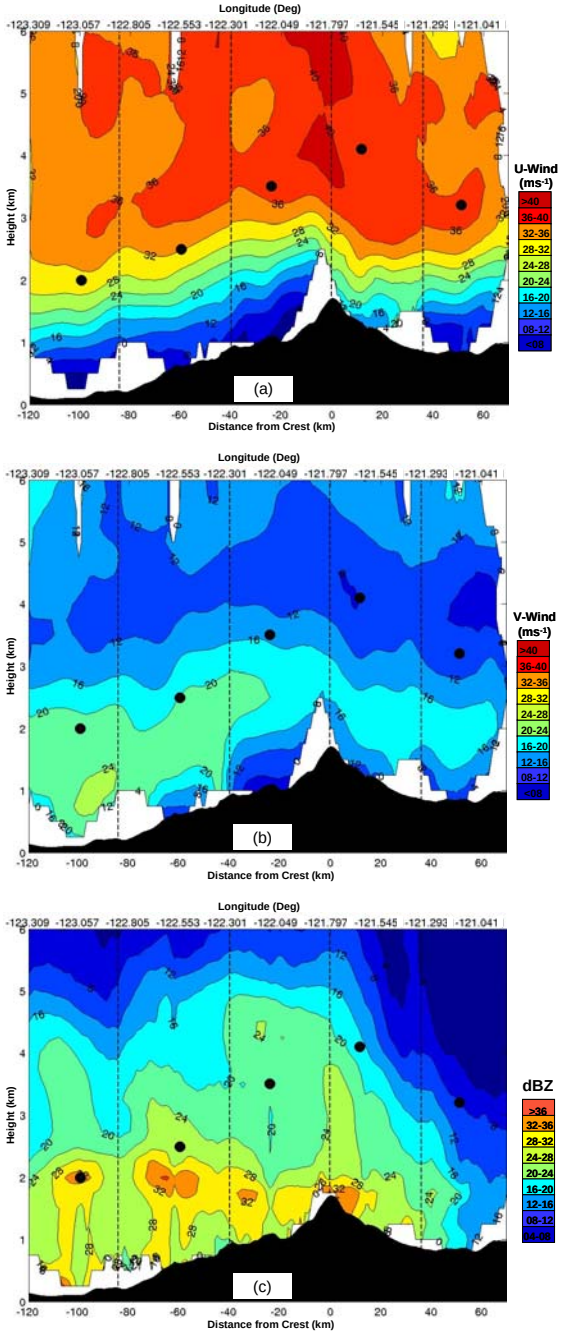


Figure 3. Average E-W cross section from airborne dual-Doppler composite grid of (a) U-component and (b) V-component flow (color shading, m $s^{-1}$). (c) Same average cross section with reflectivity (color shading, dBZ) Black dots in represent the position of P3 north-south leg. Dashed lines delineate the boundaries separating individual Doppler analysis grids included in the composite.

contours of the cross-barrier flow intersected with the mountain slope and momentum in this zone was re-directed to become virtually parallel to the mean rest immediately above the windward slopes. Above the shear layer, a jet of stronger (>36 m $s^{-1}$) flow was evident between 3-4 km, beginning 90-km upstream of the mean crest. This jet strengthened as it approached the crest, reaching speeds greater than 40 m $s^{-1}$ .

Strong V-flow was near the surface in the lower 2-km, and decreased with height above this layer (Fig. 3b). There was evidence of reduced V-component winds close to the higher terrain of the crest between -40 and -20 km upstream of the crest. The absence of a clearly defined V-maximum (or ``barrier jet'') over the windward slopes further distinguishes this IMPROVE case from aforementioned examples of profoundly blocked flow adjacent to taller mountain ranges such as the Sierras and the Alps.

### *3.2 Crest and Lee*

The extension of radar-detectable precipitation to the lee of the Cascade crest presents a unique opportunity to examine the strength and amplitude of a standing mountain wave over a mountain barrier. Once the elevated jet of strong westerly-component flow surmounted the Cascades, observations showed the high momentum air plunging downward in the immediate lee of the crest (Fig. 3a). The observed 32 m $s^{-1}$ contour, which approximately delineates the top of the shear layer, dropped from a maximum height of 3.0 km just upstream of the crest to 2.1 km [1.0 km above ground level (AGL)] approximately 10 km downstream of the crest (Fig. 3a). The 32 m $s^{-1}$ contour then rebounded slightly, before remaining steady at about 2.2-km. Independent ground-based observations at this time indicated strong winds reaching the surface, with reports of downed trees in the immediate lee of the crest (Medina et al. 2005). The positive perturbations of the U-flow in the lee of the mountain crest are consistent with properties of a vertically-propagating mountain wave (Durran 2003).

## 4. OBSERVED REFLECTIVITY PATTERNS

### *4.1 Larger scale (>20 km) Precipitation Features*

An average E-W cross section of reflectivity was also constructed from the composite Doppler radar analysis (Fig. 2b) and is shown in Fig 3c. A distinct bright-band maximum in the reflectivity field delineating the melting layer descended from 2 km over the Willamette valley to a height of 1.5 km immediately adjacent to the high terrain - an indication of cooler air banked up against the Cascade crest. Radar reflectivity decreased rapidly downstream of the crest, suggestive of large evaporation rates or precipitation fallout. Over the windward slopes, increased elevated reflectivity values were found over the Willamette valley (~100-km upstream of the crest), over the windward foothills (centered ~70-km upstream of the crest), and within a broader area

commencing ~40-km upstream of the crest and extending into the lee. Analysis of contemporaneous ground-based radar observations from S-Pol (not shown) indicates that these were relatively persistent throughout the period encompassed by the composite airborne Doppler analysis. These stationary features will be further examined with the use of a mesoscale model simulation in Part-II (Garvert et al. 2005c).

### *4.2 Smaller scale (<20 km) Precipitation Features*

Thus far the paper has emphasized the larger-scale precipitation and vertical velocity perturbations (horizontal length scales > 20-km) appearing within a meridionally-averaged E-W cross section spanning the Cascade crest. Yet as Garvert et al. (2005a,b) indicated, the strong southerly component at low-levels had significant impacts on CLW amounts at smaller scales (<20 km) as it interacted with locally complex terrain corrugations extending west from the Cascade crest within the windward-slope region.

Doppler-derived vertical velocities overlaid on the V-component flow field within an N-S section closely paralleling leg-2 of the P-3's flight track (Fig. 4a). Crude dual-Doppler estimates of vertical air motion (w) were derived by downward integration of the anelastic continuity equation subject to a boundary condition of w=0 immediately above echo top. Corroboration of these w estimates by independent observational measures (and as will be seen in Part-II, simulation results) lends increased confidence in their validity at least in a qualitative sense. These patterns provide rudimentary information on the amplitude and phase of these smaller-scale features in three-dimensional space.

In conjunction with the layer of strongly-sheared cross-barrier (U-component) flow seen in Fig. 3a, the strength of the V-flow component approached 30 m $s^{-1}$ below 3 km. As this strong flow impinged upon corrugations within the underlying foothill terrain, vertical velocity perturbations seen in the in situ flight level data (Garvert et al. 2005a) were clearly evident in the Doppler-derived flow pattern as well. Due to the rudimentary calculations and boundary conditions applied to derive the vertical velocity, the w-values can only be viewed qualitatively. Yet despite the boundary conditions of w=0 at echo top, positive w values of greater than 0.2 m $s^{-1}$ were registered at heights of 5 km, indicating the significant upward penetration of these small-scale mountain waves generated over the Cascade foothills.

In the case of the steepest and widest ancillary ridges radiating westward from the Cascade crest (viz. terrain features located between 30-40 km and 70-80 km in Fig. 4a) localized acceleration of the V-component flow was noted in the lee (i.e. north) of the local peaks. The presence of such lee accelerations collocated with negative w perturbations (Fig. 4a), is consistent with theoretically-predicted behavior of vertically propagating wave behavior (Durran 2003).

To illustrate the impact of the vertical perturbations on precipitation development, Fig. 4b displays Doppler-derived vertical velocity overlaid on reflectivity along leg-2. Consistently high dBZ values were located at a height 1.8-km in conjunction with the bright band marking the melting layer. Reflectivity enhancements were also located 5-8 km north of the individual updraft regions. For example, at 15-km from the southernmost edge of the cross section and near a height of 2.0-km, a strong vertical velocity maximum (w = 1.5 m $s^{-1}$) was evident near the location where the strong V-component flow impinged upon a 1-km high ridge. At a distance 5-8 km north of this positive vertical velocity perturbation, an enhancement in the dBZ values was observed, implying increased precipitation rates triggered by this ascent.

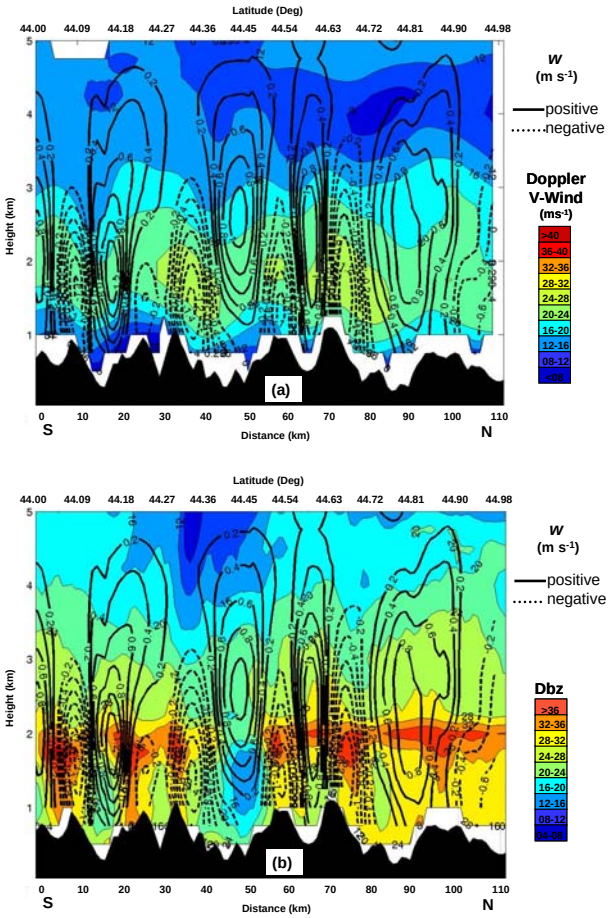


Figure 4. N-S cross-section of airborne dual-Doppler measured (a) V-component flow and (b) reflectivity along leg-2 of the P3 flight track (cf. Fig 1a). Contours of Doppler-derived vertical velocity are displayed at intervals of 0.2 m $s^{-1}$. Negative contour values are dashed.

## 5. CONCLUSION

This paper illustrates the utility of airborne dual-Doppler radar observations collected over complex orography to specify details of terrain- modified airflow and precipitation patterns at a level of detail suitable for output evaluation from state-of-the-art mesoscale models. A detailed yet horizontally comprehensive analysis of airflow and reflectivity fields during a heavy precipitation event over the central Oregon Cascades on 13-14 December 2001 has been presented. These observations were systematically collected on both sides of a major mountain barrier (viz. the Cascade range of central Oregon), and provide a unique opportunity to compare detailed kinematic measures of terrain-induced perturbations over complex terrain with a high resolution mesoscale model simulation.

This paper expands on previous 13-14 December 2001 IMPROVE studies (Garvert et al. 2005a.b, Colle et al. 2005, Woods et al. 2005, Medina et al. 2005) by providing a fully three-dimensional, uninterrupted view of reflectivity and kinematic fields spanning the complex terrain of the Cascades extending from the Willamette Valley to the lee slopes. Part-II of this study (Garvert et al. 2005c) will present results from the National Center for Atmospheric Research (NCAR) /Pennsylvania State University (PSU) Mesoscale Model (MM5), which are evaluated alongside the dual-Doppler observations and exploited to further explore the structure and evolution of these standing waves.

Additional information on the IMPROVE-project and related papers can be found at ***http://improve.atmos.washington.edu/***

## 5. ACKNOWLEDGEMENTS

This research was funded by the National Science Foundation.

## 6. REFERENCES

Bousquet, O. and B. F. Smull 2003a: Airflow and precipitation fields within deep Alpine valleys observed by airborne Doppler radar. *J. Appl Meteor.*, **42**, 1497-1513

_____ and B. F. Smull 2003b: Observations and impacts of upstream blocking during a widespread precipitation event. *Quart. J. Roy. Meteor.*, **129**, 391-409

Colle B, M. F. Garvert, J. Wolfe, C. F. Mass, and C. Woods 2005: 13-14 December 2001 IMPROVE-2 Event. Part-3. Microphysical Budgets and Sensitivity Studies*, J. Atmos. Sc*i. (IMPROVE Special Issue), In Press.

D. Durran, 2003: Lee waves and mountain waves. *Encyclopedia of Atmospheric Sciences,* Elisver Science Ltd.

Frush, C.L., P.H. Hildebrand, and C. Walther, 1986: The NCAR airborne Doppler radar. Part II: System design considerations. *23rd Radar Meteorology Conference,* AMS, 151-154, Snowmass CO

Garvert, M. F., B. A. Colle, and C. F. Mass, 2005a: The 13-14 December 2001 IMPROVE-2 Event. Part 1: Synoptic and mesoscale evolution and comparison with a mesoscale model simulation. *J. Atmos. Sci.* (IMPROVE Special Issue),In Press.

_____ ., C.P. Woods,B. A. Colle, C. F. Mass, P.V. Hobbs, M.P. Stoelinga and J. Wolfe 2005b: The 13-14 December 2001 IMPROVE-2 Event. Part 2:.: Comparisons of MM5 Model Simulations of Clouds and Precipitation with Observations *J. Atmos. Sci.* (IMPROVE Special Issue), IN Press.

_____B. Smull, C F. Mass 2005c, Mountain wave structures occurring within a major orographic precipitation event: Part II. Evaluation of mesoscale model simulations:. *32rd Conference on Radar Meteorology,* AMS, Albuquerque, NM

Jorgensen, D.P. and B.F. Smull 1993: Mesovortex circulations seen by airborne Doppler radar within a bow-echo mesoscale convective system. *Bull Amer. Meteor. Soc*., **74**, 2146-2156

Marwitz, 1987; Deep orographic storms over the Sierra Nevada. Part I. Thermodynamic and kinematic structure. *J. Atmos. Sci.,* **44,** 159-173.

Medina S., B. Smull, R.A. Houze, M. Steiner 2005: Cross Barrier Flow During Orographic Precipitation Events: Results from MAP and IMPROVE. *J. Atmos. Sci.* (IMPROVE Special Issue),In Press.

Stoelinga, M., P. V. Hobbs, C. F. Mass, J. D. Locatelli, B. A. Colle, and co-authors, 2003: Improvement of microphysical parameterizations through observational verification experiments (IMPROVE). *Bull. Amer. Meteor. Soc*., **84,** 1807-1826.

Woods, C. P., M. T. Stoelinga, J. D. Locatelli, and P. V. Hobbs, 2005: Microphysical Processes and Synergistic Interaction between frontal and orographic forcing of precipitation during the December 13, 2001 IMPROVE-2 event over the Oregon Cascades. *J. Atmos. Sci.* (IMPROVE Special Issue), In Press.

Yu, C.K. and B. F. Smull, 2000: Airborne observations of a landfalling cold front upstream of steep coastal orography. *Mon. Wea. Rev*, **128**, 1577-1603,